

Seismic structure of the Iceland mantle plume

Cecily J. Wolfe*, Ingi Th. Bjarnason†, John C. VanDecar* & Sean C. Solomon*

* Department of Terrestrial Magnetism, Carnegie Institution of Washington, 5241 Broad Branch Road, NW, Washington DC 20015, USA

† Science Institute, University of Iceland, Reykjavik, Iceland

Oceanic hotspots are generally accepted to be the manifestations of plumes of hot, upwelling mantle material^{1,2}, but the nature of such flows remains enigmatic. Iceland, for example, is one of the most thoroughly investigated hotspots, yet previous seismological^{3–5} and geodynamic^{6–12} studies have been unable to constrain the width or temperature of the plume. Here we report the results of a regional broadband seismic experiment undertaken to determine the three-dimensional velocity structure of the upper mantle beneath Iceland using relative travel times of body waves from teleseismic earthquakes. Inversion solutions of the data show a cylindrical zone of low P- and S-wave velocities that extends from 100 km to at least 400 km depth beneath central Iceland. The radius of the low-velocity anomaly is about 150 km, and its magnitude is approximately 2% for P waves and 4% for S waves, indicating that Iceland is underlain by a hot, narrow plume of upwelling mantle.

Although the interaction between the Iceland plume and the Mid-Atlantic Ridge (MAR) has several evident manifestations, a detailed understanding of that interaction has been elusive. The Iceland hotspot generates a broad topographic high⁶, thicker than normal crust¹³, and a pronounced geochemical⁷ anomaly that extends along the adjacent Reykjanes ridge. Neovolcanic zones within Iceland, interpreted as on-land extensions of the MAR, have similarities to oceanic spreading centre segments (Fig. 1). On the basis of the excess crustal thickness^{8,9}, topographic anomaly^{9,10} and rare-earth element patterns⁹, kinematic models for mantle flow beneath Iceland and the Reykjanes ridge suggest a narrow plume radius (100 km) and a significantly hotter temperature ($\Delta T = 200^\circ\text{C}$) than the surrounding mantle. In contrast, recent three-dimensional variable-viscosity models of the dynamics of mantle flow and melting beneath this ridge-centred hotspot demonstrate that a much broader (300 km radius) and cooler ($\Delta T = 75^\circ\text{C}$) plume can match the observed topographic and gravity anomalies^{11,12}. Whether the shallow horizontal component of mantle flow is radially symmetric about the hotspot centre^{11,12,14} or is channelled along the Reykjanes ridge axis^{6,9,10} has not been ascertained. Global seismological models^{3,4} display lower than average shear velocities in the upper mantle surrounding Iceland, but the lateral resolution of such models is no better than $\sim 1,000$ km. Tryggvason *et al.*⁵ inverted arrival times of teleseismic P waves recorded on an unevenly distributed network of short-period analogue seismic stations and found a narrow low-velocity anomaly in the upper 400 km beneath central Iceland, but the structure and magnitude of the anomaly were poorly constrained.

ICEMELT¹⁵ is a regional broadband seismic experiment, initially undertaken by the Carnegie Institution of Washington and now run in cooperation with the Science Institute of the University of Iceland, designed to determine the detailed upper-mantle structure beneath a mid-ocean-ridge hotspot. The ICEMELT network, installed during 1993–95 and in operation until autumn 1996, consists of 15 portable broadband, three-component STS-2 seismometers distributed throughout Iceland (Fig. 1). Relative delay times of filtered P and S waves from teleseismic earthquakes have been measured¹⁵ with a multichannel cross-correlation technique¹⁶. The resulting set of delay times is of high accuracy (standard errors

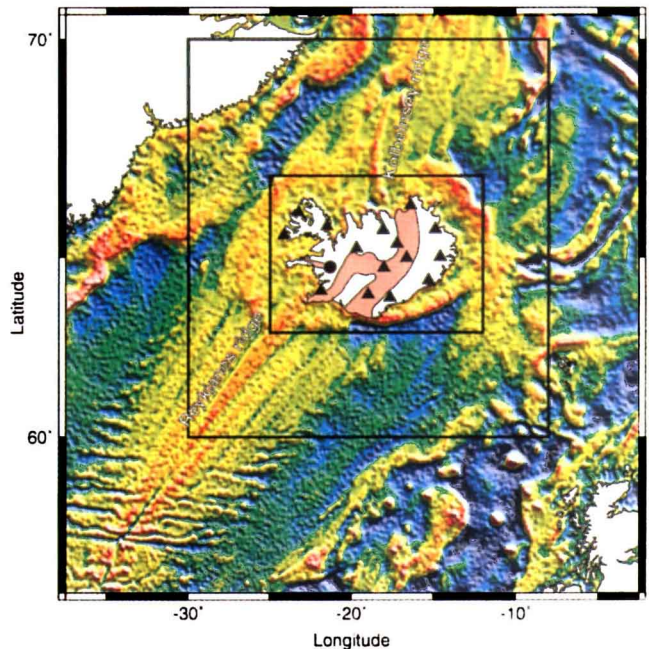


Figure 1 Location of ICEMELT seismic stations (filled triangles) within Iceland. We have also used data from the Global Seismographic Network station BORG in western Iceland (filled circle). The regional setting is illustrated by the satellite-derived gravity field²⁹ of the North Atlantic; yellow-to-red colours indicate more positive gravity values, while green-to-blue colours indicate more negative values. Positive gravity anomalies generally coincide with shallower than normal sea floor. Icelandic neovolcanic zones are shaded in red. The outer and inner rectangles represent respectively the exterior boundary, in map view, of the seismic velocity grid used for delay-time inversion and the interior boundary where the best resolution is obtained and within which we confine our interpretations. The model grid extends from 0 to 1,000 km in depth.

of ~ 30 ms for P waves and ~ 100 ms for S waves). As described by Bjarnason *et al.*¹⁵, there is a consistent qualitative pattern for measured body-wave delays, which indicates a narrow low-velocity anomaly throughout the upper mantle beneath central Iceland: P and S waves that travel through this region are significantly delayed relative to waves traversing other paths.

Here P- and S-wave delays are independently used to solve for three-dimensional velocity structure, earthquake relocations and station terms by means of a robust nonlinear, regularized travel-time inversion scheme¹⁷. Because these types of problems are inherently underdetermined, this method searches for the minimum-structure model required to satisfy the data by minimizing spatial gradients and roughness. The inversions incorporate relative arrival times of 601 P waves from 86 earthquakes (including 12 earthquakes with core phases) and 560 S-wave times from 78 earthquakes (including 13 earthquakes with core phases). The earthquakes employed in this study are well distributed in azimuth around Iceland (see Supplementary Information). The dominant seismic wavelengths are ~ 10 km for the P waves and 50–75 km for the S waves.

The inversion solutions, with one nonlinear iteration to incorporate ray bending effects, are shown in Fig. 2 as percentage velocity perturbations to a standard radial Earth model¹⁸. Our models explain 95% of the root-mean-squared (r.m.s.) residual for P-wave delay data (from 0.4 to 0.02 s) and 91% of that for S-wave data (from 1.4 to 0.05 s), with final r.m.s. values slightly smaller than our *a priori* estimates of data errors. Because the station spacing is ~ 75 km and incidence angles of teleseismic waves steepen in the shallowest mantle, there are no crossing wave paths above ~ 100 km depth¹⁷. Velocity structure is thus poorly constrained at these shallow depths, although the station terms shown in Fig. 2 account

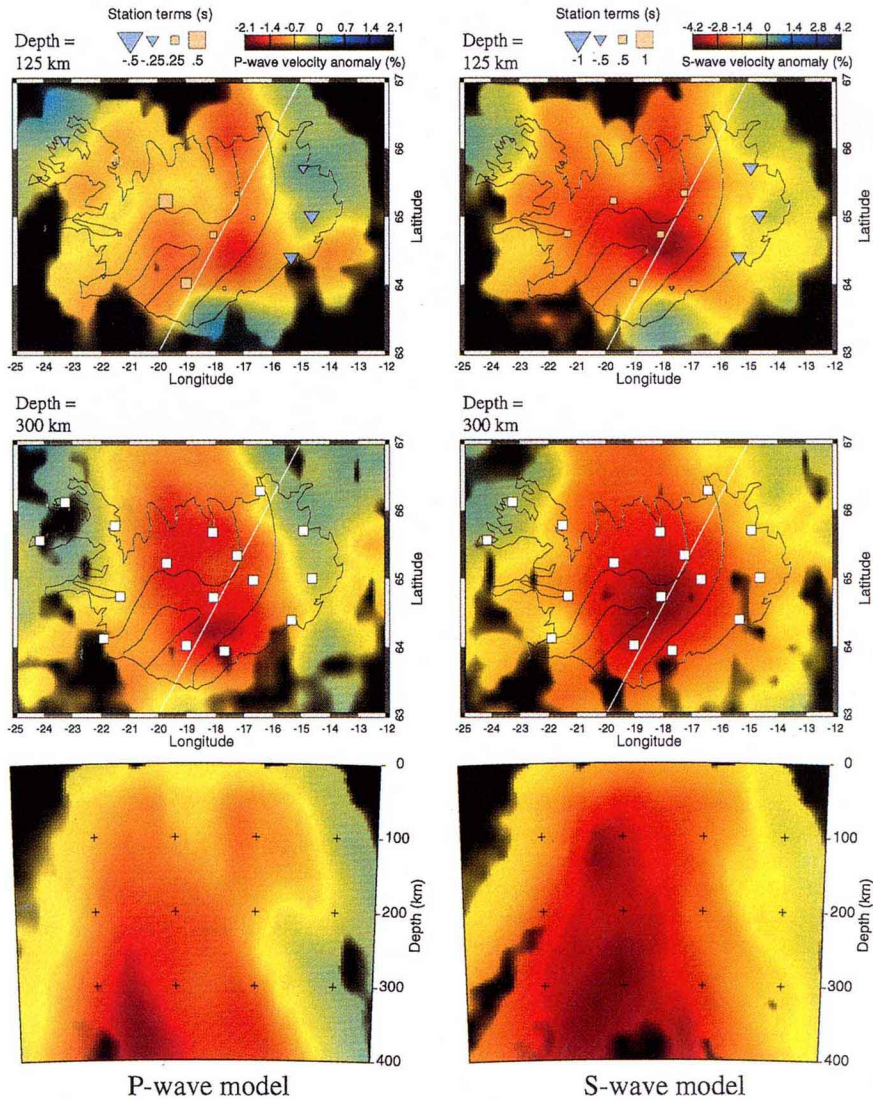


Figure 2 Cross-sections through the P-wave (left-hand column) and S-wave (right-hand column) models. Within this region, velocity nodes are spaced at 25 km in depth, 0.5° in longitude and 0.25° in latitude. Velocity perturbation models are shown in map view at depths of 125 km (top row) and 300 km (middle row); vertical cross-sections (bottom row) are along the white line in map views. The velocity perturbations shown are relative variations across the modelled volume; the absolute velocities are unconstrained. Yellow-to-red colours represent low-velocity anomalies: regions with sparse coverage are faded to black. Station locations are shown as white squares in the middle row. Square and triangular

symbols in the top row indicate the magnitude and sign of the station terms. The inversions solve simultaneously for independent (undamped) station terms to absorb as much shallow structure as possible into these terms and to avoid projecting such structure into the underlying velocity model. These station-term times represent the vertical travel-time of waves associated with each station and thus account in part for the integrated differences in mantle structure above 100 km depth, combined with the effects of crustal thickness variations and differences in station elevation. The Icelandic coastline and neovolcanic zone boundaries are shown as black lines.

in part for the integrated differences in mantle structure above 100 km depth, combined with the effects of crustal thickness variations and differences in station elevation.

The most prominent feature in our inversion solutions is a low-velocity anomaly beneath central Iceland extending down to at least 400 km depth (Fig. 2). At 300 km depth, the low-velocity anomaly is approximately circular and 150–200 km in radius (defined by the region at which the perturbation drops below $1/e$ of the maximum value). At 125 km depth, in contrast, the low-velocity region coincides more nearly with the surface expression of the neovolcanic zone, the correlation being most evident in northern Iceland. The centre of the low-velocity region is vertically continuous and does not show significant lateral shifts over the depth range 100–400 km (Fig. 2), in contrast to previous P-wave images of Tryggvason *et al.*⁵ that suggested a more variable structure. We note, however, that these previous results achieved only an 18% reduction

in r.m.s. delays (from 0.46 to 0.38 s)⁵, suggesting that larger errors for the travel times obtained from analogue recordings may have influenced the model.

We have performed a number of resolution tests (see Supplementary Information), which indicate that the basic geometry of both the circular low-velocity anomaly throughout the depth range 100–400 km and the shallower (<150 km) low-velocity anomaly extending along the neovolcanic zones are both well resolved. These tests demonstrate that the inversion solutions (Fig. 2) cannot be produced by either a significantly shallower (≤ 200 km depth) or a broader (300 km radius) low-velocity anomaly. Inversions in which the depth extent of the velocity anomaly is constrained to be less than 400 km do not satisfy the data as well as models that allow deeper structure. In general, the resolution tests show that a narrow, cylindrical slow region extending throughout the Icelandic upper mantle will appear broadened (by as much as 50%) in the inversion

solutions, but there should be no significant artificial widening with depth. These tests also indicate that the magnitudes of the velocity anomalies in the inversion solutions are probably underestimated (we retrieve 75% of the velocity anomaly for the central plume structure). At seismic frequencies, the anomaly magnitude could be further reduced by wavefront healing¹⁹, where rays diffract around the edge of a low-velocity anomaly and arrive before the Fermat ray, reducing the observed time delay by an amount that depends on several factors, including the seismic wavelength, the distances of the wave path from the velocity anomaly and the anomaly magnitude²⁰. Taking into consideration all of these effects, the imaged velocity anomalies (Fig. 2) should be regarded as providing minimum values for the magnitude of the velocity perturbations beneath Iceland and a maximum value for the width of the central low-velocity anomaly.

Our P- and S-wave models are generally similar in structure (Fig. 2), but the magnitude of the anomaly is substantially larger for the S-wave model (4%) than for the P-wave model (2%). We have confirmed this S-to-P anomaly ratio in the raw delay-time data. The relative delays of P and S waves at pairs of stations from common earthquake sources are correlated, with the S delays generally four times larger than the P delays. This ratio is approximately a factor of two larger than if the fractional variations in velocity were equal for P and S waves. There is some difference between the P and S velocity structures beneath central Iceland, which is the point of minimum velocity for S waves, but not for P waves (Fig. 2). As shear-wave splitting of the order of 1–2 s has been observed at several ICEMELT stations¹⁵, mantle anisotropy could account for some of the differences in P- and S-wave models. In particular, a narrow zone of upwelling flow beneath central Iceland would tend to induce vertical alignment of the crystallographic *a*-axes of mantle olivine crystals, which would produce a vertically oriented fast direction of anisotropy for P waves but not for S waves²¹. Our P- and S-wave models also indicate some asymmetry in the integrated structure above 100 km depth, as shown in both the station terms and shallowest mantle structure (Fig. 2), suggesting that the integrated travel times for shallow structure beneath stations on older crust (>7 Myr; ref. 22) along the eastern coast are fast relative to stations on older crust in western Iceland. When combined with the recent observation of the relatively large 35-km crustal thickness in eastern Iceland²³, these results suggest that beneath eastern Iceland the mantle shallower than 100 km displays the highest average wave speeds in the region.

The low-velocity anomaly in the upper mantle beneath Iceland can be interpreted as the locus of the active plume and its interaction with the spreading plate boundary. (Note that we cannot constrain the structure outside of the imaged region, so the full areal extent of mantle affected by the Iceland hotspot remains unknown.) The imaged location of the centre of the plume is broadly similar to the zone of highest ³He/⁴He concentrations within the neovolcanic zones²⁴, which has previously been suggested to mark the region of greatest plume influence. The seismic images indicate that the Iceland mantle plume persists down to at least 400 km depth. Although our data cannot resolve the signature of the plume at greater depth, observations of P-to-S conversions from upper-mantle discontinuities beneath Iceland are consistent with elevated temperatures and upwelling flow in the depth interval 400–700 km (ref. 25).

The maximum velocity anomalies can be converted to a contrast in temperature ΔT between the plume and surrounding mantle, on the basis of laboratory measurements of the temperature derivatives of wave speeds in olivine²⁶. The P- and S-wave anomalies yield ΔT values of 300 and 600 °C, respectively. The significantly larger magnitude of ΔT estimated from the S-wave model could reflect several influences not taken into account in this simple conversion, including the presence of melt²⁷, anelasticity²⁸ and anisotropy²¹. Accounting for the effect of anelastic dispersion²⁸, for instance, gives lower ΔT values of 200 °C for P waves and 300 °C for S waves, results more consistent with previous estimates for Iceland^{8–10,12,13}. Further

analysis of other seismic phases (for example, surface waves, shear-wave splitting) will be necessary to determine the relative importance of anisotropy, anelasticity and melt on the velocity structure.

Both the P- and S-wave images nonetheless provide strong support for the model^{8–10} of a hot and narrow plume beneath central Iceland having a vertical extent of at least 400 km, and against the model of a relatively cool, broad plume, predicted by several recent numerical models^{11,12}. These numerical studies however, indicate that a narrow plume significantly overpredicts the crustal thickness beneath Iceland and the elevation contrast between Iceland and the adjacent mid-ocean ridge. A possible means for reconciling the seismic observation of a narrow Icelandic plume with the results of flow models^{11,12} is the horizontal channelling of plume-derived melts down the nearby ridge^{6,12}. □

Received 1 July; accepted 4 December 1996.

- Wilson, J. T. *Sci. Am.* **208**, 86–100 (1963).
- Morgan, W. J. *Nature* **230**, 42–43 (1971).
- Zhang, Y.-S. & Tanimoto, T. *J. Geophys. Res.* **98**, 9793–9823 (1993).
- Grand, S. P. *J. Geophys. Res.* **99**, 11591–11621 (1994).
- Tryggvason, K., Husebye, E. S. & Stefánsson, R. *Tectonophysics* **100**, 94–118 (1983).
- Vogt, P. R. *Nature* **240**, 338–342 (1972).
- Schilling, J.-G. *Nature* **242**, 565–571 (1973).
- McKenzie, D. *J. Petrol.* **25**, 713–765 (1984).
- White, R. S., Bown, J. W. & Smallwood, J. R. *J. Geol. Soc. Lond.* **152**, 1039–1045 (1995).
- Schilling, J.-G. *Nature* **352**, 397–403 (1991).
- Ribe, N. M., Christensen, U. R. & Theissing, J. *Earth Planet. Sci. Lett.* **134**, 155–168 (1995).
- Ito, G., Lin, J. & Gable, C. W. *Earth Planet. Sci. Lett.* **144**, 53–74 (1996).
- Bjarnason, I. Th., Menke, W., Flóvenz, Ó. G. & Caress, D. *J. Geophys. Res.* **98**, 6607–6622 (1993).
- Feighner, M. A., Kellogg, L. H. & Travis, B. J. *J. Geophys. Res. Lett.* **22**, 715–718 (1995).
- Bjarnason, I. Th., Wolfe, C. J., Solomon, S. C. & Gudmundson, G. *J. Geophys. Res. Lett.* **23**, 459–462 (1996); *Geophys. Res. Lett.* **23**, 903 (1996).
- VanDecar, J. C. & Crosson, R. S. *Bull. Seismol. Soc. Am.* **80**, 150–169 (1990).
- VanDecar, J. C., James, D. E. & Assumpção, M. *Nature* **378**, 25–31 (1995).
- Kennett, B. L. N. & Engdahl, E. R. *Geophys. J. Int.* **105**, 429–465 (1991).
- Wielandt, E. in *Seismic Tomography* (ed. Nolet, G.) 85–98 (Reidel, Dordrecht, 1987).
- Nataf, H.-C. & VanDecar, J. *Nature* **364**, 115–120 (1993).
- Kendall, J.-M. *Geophys. Res. Lett.* **21**, 301–304 (1994).
- Saemundsson, S. *Jökull* **29**, 7–28 (1979).
- White, R. S. *et al. Eos* **77**, 197, 200–201 (1996).
- Kurz, M. D., Meyer, P. S. & Sigurdsson, H. *Earth Planet. Sci. Lett.* **74**, 291–305 (1985).
- Shen, Y., Solomon, S. C., Bjarnason, I. Th. & Purdy, G. M. *Geophys. Res. Lett.* **23**, 3527–3530 (1996).
- Isaak, D. G. *J. Geophys. Res.* **97**, 1871–1885 (1992).
- Faul, U. H., Toomey, D. R. & Waff, H. S. *Geophys. Res. Lett.* **21**, 29–32 (1994).
- Karato, S. *Geophys. Res. Lett.* **20**, 1623–1626 (1993).
- Smith, W. H. & Sandwell, D. T. *Eos* **76**, 156 (1995).

Supplementary Information is available on Nature's World-Wide Web site (<http://www.nature.com>) or as paper copy from Mary Sheehan at the London editorial office of Nature.

Acknowledgements: We thank Björn Bjarnason, Birgir Bjarnason, Bryndís Brandsdóttir, Haukur Brynjólfsson, Kristinn Egilsson, Gunnar Gudmundson, Eythór Hannesson, Tryggvi Hardarson, Lárus Helgason, Bogi Ingimundarson, Haraldur Jónsson, Einar Kjartansson, A. Kuehnel, R. Kuehnel, Pálmi Sigurdsson, Ragnar Thrudmarsson, and the staff of the National Electric Company of Iceland (Landsvirkjun) for assistance with station installation and maintenance; the IRIS-DM5 for making available data from the Global Seismographic Network station BORG; W. Menke for discussions; and N. Ribe for comments. This work was supported by the US NSF.

Correspondence should be addressed to C.J.W. (e-mail: cecily@dtm.ciw.edu).

Nest and egg clutches of the dinosaur *Troodon formosus* and the evolution of avian reproductive traits

David J. Varricchio*, Frankie Jackson†, John J. Borkowski‡ & John R. Horner†

* Old Trail Museum, PO Box 919, Choteau, Montana 59422, USA

† Museum of the Rockies, Montana State University, Bozeman, Montana 59717, USA

‡ Department of Mathematical Sciences, Montana State University, Bozeman, Montana 59717, USA

Living archosaurs (crocodilians and birds) share several reproductive features, including hard-shelled eggs¹, parental care^{2,3}, assembly-line oviducts⁴ and luteal morphology⁵. Nevertheless, crocodilians produce many small eggs that they ovulate, shell